Phosphorescence and Optically Detected Magnetic Resonance Investigation of the Binding of the Nucleocapsid Protein of the Human Immunodeficiency Virus Type 1 and Related Peptides to RNA[†,⊥]

Wai-Chung Lam,[‡] August H. Maki,[*,‡] Jose R. Casas-Finet,[§] John W. Erickson,[§] Bradley P. Kane,[∥] Raymond C. Sowder, II,[∥] and Louis E. Henderson[∥]

Department of Chemistry, University of California, Davis, California 95616, and Structural Biochemistry Program and AIDS Vaccine Program, Program Resources Inc./DynCorp., National Cancer Institute–Frederick Cancer Research and Development Center, Frederick, Maryland 21702

Received April 21, 1994; Revised Manuscript Received June 30, 1994[⊗]

ABSTRACT: The RNA and DNA complexes of nucleocapsid protein p7·Zn (NCp7·Zn) of the human immunodeficiency virus type 1 (HIV-1) are studied by phosphorescence and optically detected magnetic resonance (ODMR). The single tryptophan, Trp37, which is located on the C-terminal zinc finger domain is used as an intrinsic probe. Reductions in the triplet state zero-field splitting (zfs) *D* parameter of Trp37 upon complex formation with poly(I) and poly(U) are observed. These results, in conjunction with the phosphorescence red-shifts and triplet state lifetime reductions that are observed, suggest the presence of aromatic stacking interactions between NCp7·Zn and the bases of the RNA polymers. An alteration of the intersystem crossing pattern upon complex formation, in addition to the above mentioned spectroscopic shifts, also is consistent with previously observed tryptophans that undergo stacking interactions with DNA bases [Zang, L.-H., Maki, A. H., Murphy, J. B., & Chase, J. W. (1987) *Biophys. J. 52*, 867–872. Tsao, D. H. H., Casas-Finet, J. R., Maki, A. H., & Chase, J. W. (1989) *Biophys. J. 55*, 927–936]. These conclusions support those from a recent ODMR study [Lam, W.-C., Maki, A. H., Casas-Finet, J. R., Erickson, J. W., Sowder, R. C., II, & Henderson, L. E. (1993) *FEBS Lett. 328*, 45–48] of NCp7·Zn binding to 5-mercurated polyuridylic acid [poly(5-HgU)] in which stacking interactions between the RNA and NCp7·Zn are inferred from the observation of an external heavy atom effect induced on Trp37. The extent of the spectroscopic effects observed varies with different RNA complexes; the phosphorescence red-shifts, for instance, correlate with the affinities of NCp7·Zn for various RNA bases as measured by fluorescence quenching experiments [Casas-Finet, J. R., Sowder, R. C., II, Sakaguchi, K., Appella, E., Henderson, L. E., & Erickson, J. W. (1993) *Biophys. J. 64*, A178]. The complexes of an 18mer synthetic second zinc finger peptide of NCp7 with RNA polymers gave results similar to NCp7·Zn, indicating that tryptophan in either the wild type protein or in the synthetic peptide experience similar environments. However, spectroscopic effects of smaller magnitude are observed in the synthetic second zinc finger peptide complexes, relative to those in the NCp7·Zn complexes, suggesting that the two zinc fingers in NCp7·Zn may act in concert to bind RNA. A synthetic carboxymethylated second zinc finger peptide in which a zinc finger structure cannot be formed also is studied. The triplet state properties observed for the uncomplexed synthetic carboxymethylated second zinc finger peptide are similar to those of the noncarboxymethylated synthetic second zinc finger peptide, suggesting that the tryptophans in the two fingers have similar environments in the uncomplexed form. When either poly(I) or poly(U) is added to the synthetic carboxymethylated second zinc finger peptide, practically no spectroscopic effects are observed, indicating weak or no interaction between Trp37 and the RNAs under experimental conditions similar to those used for NCp7·Zn and the synthetic second zinc finger peptide binding.

The viral genome of the human immunodeficiency virus type 1 (HIV-1[1]), as in all retroviruses, contains *pol*, *env*, and *gag* regions. The Gag proteins are known to play a structural role in the virus. After translation, the Gag and Gag-Pol precursor function in viral assembly and budding to form the initial immature particle. During maturation, the Gag precursor is cleaved by HIV protease into six products (p17-p24-p2-p7-p1-p6) (Henderson et al., 1992). The nucleocapsid protein p7·Zn (NCp7·Zn) domain in the precursor is important for viral RNA encapsidation and packaging (Gorelick et al., 1990). In the mature virus, the NCp7·Zn protein complexes

[†] This research was partially supported by NIH Grant ES-02662 (A.H.M.).

[⊥] The content of this publication does not necessarily reflect the views or policies of the Department of Health and Human Services, nor does mention of trade names, commercial products, or organization imply any endorsement by the U.S. Government.

[*] Author to whom correspondence should be addressed.

[‡] Department of Chemistry, University of California.

[§] Structural Biochemistry Program, National Cancer Institute–Frederick Cancer Research and Development Center.

[∥] AIDS Vaccine Program, National Cancer Institute–Frederick Cancer Research and Development Center.

[⊗] Abstract published in *Advance ACS Abstracts,* August 1, 1994.

[1] Abbreviations: dG_8, deoxyguanylic acid octamer; *E. coli*, *Escherichia coli*; *E. coli* SSB, *Escherichia coli* single-stranded DNA binding protein; ESMS, electrospray ionization mass spectrometry; HAE, heavy atom effect; HIV-1, human immunodeficiency virus type 1; ISC, intersystem crossing; MIDP, microwave-induced delayed phosphorescence; NCp7·Zn, nucleocapsid protein p7; ODMR, optically detected magnetic resonance; POEMIDP, pulsed optical excitation microwave-induced delayed phosphorescence; poly(5-HgU), 5-mercurated polyuridylic acid; poly(A), polyadenylic acid; poly(C), polycytidylic acid; poly(dT), polydeoxythymidylic acid; poly(G), polyguanylic acid; poly(I), polyinosinic acid; poly(U), polyuridylic acid; RP-HPLC, reverse-phase high-pressure liquid chromatography; SLR, spin–lattice relaxation; zfs, zero-field splitting.

0006-2960/94/0433-10693$04.50/0

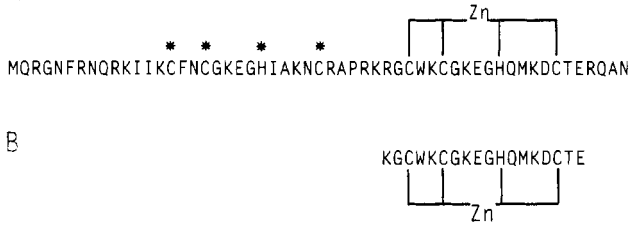

FIGURE 1: Amino acid sequence of (A) NCp7·Zn and (B) the synthetic second zinc finger peptide. The Zn coordination site in the second zinc finger is shown. The CCHC motif of the first zinc finger is indicated by asterisks. The synthetic carboxymethylated second zinc finger peptide has the same sequence as in part B but with all the cysteine residues carboxymethylated.

with RNA to form part of the internal core structure. NCp7·Zn is a small peptide (ca. 55 residues) containing two copies of a CCHC array (Cys-X_2-Cys-X_4-His-X_4-Cis, X is variable) that bind zinc quantitatively to form zinc-finger-like structures (South et al., 1990; Bess et al., 1992). The formation of the zinc finger domains are required for the correct functioning of the virus (Bess et al., 1992; Gorelick et al., 1993). Deletion of one finger or mutation of a cysteine to serine in either finger causes a decrease in RNA packaging (Gorelick et al., 1990; Sakaguchi et al., 1993). A NMR solution structure study of NCp7·Zn purified from virus containing the two zinc finger domains (Summers et al., 1992) shows that NCp7·Zn contains two structured zinc finger domains linked by a flexible peptide chain. Solution structure studies on a synthetic N-terminal zinc finger peptide bound to an oligonucleotide (South & Summers, 1993) suggest that interactions occur between the hydrophobic residues on the zinc finger domains and nucleic acid bases.

NCp7·Zn of HIV-1 has only one tryptophan, Trp37, which is located on the C-terminal zinc finger domain. The corresponding position on the N-terminal zinc finger domain is occupied by phenylalanine (Henderson et al., 1990, 1992). The sequence of NCp7·Zn is shown in Figure 1. A recent site-directed mutagenesis study to map the functionally important residues shows that the two aromatic residues in the protein, Phe16 in the N-terminal zinc finger and Trp37 in the C-terminal zinc finger, are essential for viral replication (Dorfman et al., 1993).

The triplet state of Trp37 is an intrinsic probe for phosphorescence and ODMR studies of NCp7·Zn interaction with RNA polymers. Phosphorescence and ODMR have been used successfully in the past to study many proteins and their interactions with ligands and nucleic acids (Maki, 1984; Tsao et al., 1989) and have revealed tryptophan stacking interactions. In particular, earlier studies have revealed aromatic stacking interactions between tryptophan residues of *Escherichia coli* single-stranded DNA binding protein (SSB) and ssDNA (Zang et al., 1987; Tsao et al., 1989). Details of the application of ODMR to the studies of biopolymers can be found in several reviews (Kwiram, 1982; Maki, 1984; Hoff, 1989). Interactions with RNA bases can cause changes in the environment of Trp37. If stacking interactions with RNA bases are present, red-shifts in the phosphorescence 0,0-band, reductions in triplet lifetime, and changes in the intersystem crossing (ISC) pattern, as well as changes in the triplet state zero-field splitting parameters (D and E) of Trp37 may be observed (Zang et al., 1987; Tsao et al., 1989). We reported recently, on the basis of observed heavy atom effects, that Trp37 in NCp7·Zn undergoes stacking interactions with the heavy-atom-derivatized RNA 5-mercurated polyuridylic acid [poly(5-HgU)], where the Hg is blocked by 2-mercaptoethanol to ensure no covalent interaction between the Hg and NCp7·Zn (Lam et al., 1993). Here we report measurements on various complexes between NCp7·Zn and unmodified RNAs to determine if stacking interactions are also present and to see if there is a correlation between triplet state properties and the affinities of NCp7·Zn for different RNA bases. The results of phosphorescence and ODMR measurements on NCp7·Zn and its complexes with some unmodified RNA homopolymers are reported. A correlation between spectroscopic observables and the binding affinities of NCp7·Zn for the different oligonucleotides determined from fluorescence quenching measurements (Casas-Finet et al., 1993) is also discussed. In addition, two NCp7-related synthetic peptides, 18 residue sequences similar to the C-terminal zinc finger domain (Figure 1) either unmodified or carboxymethylated at the cysteines so that a zinc finger cannot be formed, are used as models to help shed light on the details of NCp7·Zn/nucleic acid interactions.

MATERIALS AND METHODS

HIV-1/MN NCp7, synthetic HIV-1/HXB2 second zinc finger peptide (acetyl-KGCWKCGKEFHQMKDCTE-amide), and the synthetic *S*-(carboxymethyl)cysteine second zinc finger peptide homologue were obtained as follows. The coding sequence for HIV-1/MN NCp7 was cloned into a pMal-C vector (P. Powell, et al., unpublished) and expressed in *E. coli* as a maltose binding protein (MBP)-Xa-NCp7 fusion protein (where Xa represent a four residue peptide conferring a site for factor Xa proteolysis). The fusion protein was purified by disrupting *E. coli* with sonication in Tween-20. The released fusion protein was then precipitated by removal of the detergent using an organic extraction technique involving the formation of an acetonitrile layer in 0.5 M NaCl at 2 °C. The precipitate was redissolved at pH 11 and digested with factor Xa at pH 8.5. Acid precipitation of the released MBP leaves mostly p7 and nucleic acids in solution, and these were resolved by reverse-phase high-pressure liquid chromatography (RP-HPLC) using a Waters 25 × 100 mm Prep Pak μBondpak C18 RCM cartridge and an acetonitrile gradient acidified with trifluoroacetic acid (Henderson et al., 1992). A small amount of internal cleavages at arginine residues generated smaller fragments of the p7 which eluted near the p7 peak. These were removed by rechromatography on a more highly tailored gradient.

The purified NCp7 was sequenced by Edman degradation and weighed by electrospray ionization mass spectrometry (ESMS). Both methods indicated that the purified NCp7 was full length with no observable post-translational modifications. In addition, fluorescence titrations and ESMS demonstrated the ability of the purified protein to bind 2 mol equiv of zinc. The recombinant NCp7·Zn was also shown to give NMR signals that were indistinguishable from wild-type NCp7 for which the three-dimensional structure has been determined (Summers, personal communication).

The synthetic second finger peptide was synthesized and purified by Macromolecular Resources (Fort Collins, CO) and further purified by RP-HPLC. The carboxymethylated homologue was sufficiently pure and was used without rechromatography.

The lyophilized proteins were dissolved in 10 mM phosphate buffer (pH 6.5), except where noted. Polyadenylic acid [poly(A)], polycytidylic acid [poly(C)], polyguanylic acid [poly(G)], polyuridylic acid [poly(U)], oligodeoxyguanylic acid (dG_8), and polydeoxythymidylic acid [poly(dT)] were purchased from Pharmacia. Polyinosinic acid [poly(I)] was obtained from Miles Laboratories. A 5-brominated uridylic acid oligomer [$(5\text{-BrdU})_7$dT] was synthesized by Dr. Leo M

Lee at Program Resources, Inc., using phosphoramidite chemistry. The oligomer was desalted, size-purified electrophoretically, and electroluted. It was lyophilized before storage. 5-Mercurated polyuridylic acid [poly(5-HgU)] was from P.L. Biochemicals and was dissolved in 5 mM phosphate buffer, pH 6.5. Nucleic acid concentrations in terms of nucleotide bases were determined by UV absorption spectroscopy using molar extinction coefficients (in M^{-1} cm^{-1} provided in the manufacturer's 1992 catalog except where noted): ϵ_{258} = 9800, ϵ_{269} = 6200, ϵ_{248} = 10 200, ϵ_{260} = 9350, ϵ_{253} = 10 400, ϵ_{253} = 10 400, ϵ_{264} = 8520, ϵ_{278} = 6900, and ϵ_{267} = 15 000 for poly(A), poly(C), poly(I) (Pharmacia 1992 Catalog), poly(U), poly(G), dG_8, poly(dT) (Ts'o et al., 1966), $(5\text{-BrdU})_7$dT, and poly(5-HgU) (Michelson et al., 1962), respectively. Excess 2-mercaptoethanol was added to the poly(5-HgU) to prevent the formation of any covalent bonds between the Hg atom and peptide residues. The concentration of NCp7·Zn in the samples was ca. 0.25 mM in the uncomplexed protein and ca. 0.06 mM in the complexes as measured by UV absorption using ϵ_{280} = 5700. The nucleic acid concentration (in nucleotide bases) was ca. 20 times that of the tryptophan concentration in the samples. All samples contained 20% (v/v) ethylene glycol as a cryosolvent. The complexes were formed at ambient temperature by the progressive addition of an aliquot of concentrated NCp7·Zn to the nucleic acid solution, and allowed to stand for 10 min prior to phosphorescence measurements at 77 K. ODMR measurements were made at 1.2 K in order to suppress spin–lattice relaxation (SLR). Excitation was at 295 nm with 16 nm bandpass and the emission bandpass was 3 nm. The ODMR techniques have been described in detail in two reviews (Maki, 1984; Hoff, 1989), and the current experimental setup and methods have been described previously (Tsao et al., 1989).

A modified microwave-induced delayed phosphorescence (MIDP) experiment, pulsed optical excitation microwave-induced delayed phosphorescence (POEMIDP), was used in this study to determine the relative populating rates of the three triplet sublevels. The optical pulse was supplied by a mechanical shutter with a response time (opening or closing) of ca. 1 ms. The experiment is similar to a MIDP experiment (Schmidt et al., 1969) in which the sample phosphorescence is allowed to decay and the microwave frequency is swept rapidly through a resonance transition after a certain delay time, t'. The POEMIDP modification relies on a short optical excitation interval that minimizes the effects of spin–lattice relaxation (SLR) on the sublevel populations.

If excitation of the sample is extinguished at $t = 0$, and the temperature is low enough such that SLR can be neglected, then the phosphorescence intensity at $t = t'$ is given by

$$I(t') = c\sum k_s^r N_s(0)\exp(-k_s t') \quad (1)$$

where $s = x$, y, or z, $N_s(0)$ is the population of sublevel T_s at $t = 0$, k_s^r is the radiative rate constant of T_s, k_s is its overall decay constant, and c is a constant that depends on the apparatus. If (as in tryptophan) only one of the sublevels is significantly radiative (k_y^r, $k_z^r \ll k_x^r$) and if the time t' is small enough so that $k_s t' \ll 1$ for each sublevel s, then eq 1 reduces to

$$I(t') \cong ck_x^r N_x(0) \quad (2)$$

If we now suddenly induce transitions between T_x and T_u ($u = y$ or z) by microwave fast passage through the corresponding resonance line, the phosphorescence intensity after the fast passage will be

$$I'(t') \cong ck_x^r[(1-f)N_x(0) + fN_u(0)] \quad (3)$$

where f is the population transfer factor. The microwave power can be adjusted for saturation of the transition, in which case $f = {}^1/_2$. For saturation, the change in phosphorescence intensity that accompanies the fast passage is, from eqs 2 and 3,

$$\Delta I^{ux}(t') \cong {}^1/_2 ck_x^r[N_u(0) - N_x(0)] \quad (4)$$

If we divide eq 4 by eq 2, the phosphorescence intensity immediately prior to the fast passage, we get

$$\Delta I^{ux}(t')/I(t') \cong {}^1/_2[N_u(0)/N_x(0) - 1] \quad (5)$$

from which

$$N_u(0)/N_x(0) \cong 1 + 2\Delta I^{ux}(t')/I(t') \quad (6)$$

If the triplet state is populated by an optical pulse that is short relative to each sublevel lifetime, $N_s(0) \propto P_s$ (relative populating rate) so that $N_u(0)/N_x(0)$ in eq 6 can be replaced with P_u/P_x. Application of eq 6 to both transitions involving T_x ($u = y$ and z) yields the relative populating rates of all three sublevels. Thus, the validity of eq 6 depends on the following: (1) SLR is slow enough to be neglected; (2) t' is sufficiently short that $k_s t' \ll 1$ for each sublevel, and (3) only T_x is significantly radiative. Finally, the equivalence of $N_u(0)/N_x(0)$ and P_u/P_x depends on pulsed optical excitation of sufficiently short duration so that Δt (pulse) $\ll k_s^{-1}$. In practice, the presence of extraneous phosphorescence at $t = t'$, if not corrected for, will affect the accuracy of the calculated $N_u(0)/N_x(0)$. $I(t')$ will then be too large, reducing the magnitude of the second term on the right hand side of eq 6, so that the degree of spin alignment will always be underestimated.

RESULTS

Phosphorescence and Triplet Lifetime. The phosphorescence spectra of NCp7·Zn and two of its RNA complexes are shown in Figure 2. Table 1 lists the wavelengths of the phosphorescence 0,0-band peaks and triplet lifetimes of NCp7·Zn and its RNA and DNA complexes. The 0,0-band of NCp7·Zn peaks at 409.2 nm, suggesting that Trp37 is at most partially exposed (Hershberger et al., 1980). The largest spectroscopic change occurs when NCp7·Zn is bound to poly(I) (which is similar to G in nucleobase structure). The 0,0-band peak is shifted by 5.9 nm from 409.2 to 415.1 nm (Table 1), upon complex formation. Also, the major phosphorescence lifetime component is reduced from 6.5 s for the free NCp7·Zn, which is in the normal range for tryptophans, to 4.9 s in the NCp7·Zn/poly(I) complex. The NCp7·Zn/poly(G) and the NCp7·Zn/dG_8 complexes exhibit identical phosphorescence red-shifts and the lifetime reductions are similar to those of the poly(I) complex. The phosphorescence wavelength shift is somewhat less, however, than that observed for the poly(I) complex. The base G at liquid helium temperature (4.2 K or lower) emitted an intense structured phosphorescence overlapping that of Trp37, making the Trp37 phosphorescence characteristics more difficult to determine. The NCp7·Zn/poly(dT), NCp7·Zn/poly(C), and NCp7·Zn/poly(A) complexes exhibit smaller phosphorescence red-shifts and lifetime reductions. The very large lifetime reduction observed for the NCp7·Zn/$(5\text{-BrdU})_7$dT complex shows that there is an external HAE induced on Trp37 by the Br atom.

The phosphorescence spectra of the synthetic second zinc finger peptide and two of its RNA complexes are shown in

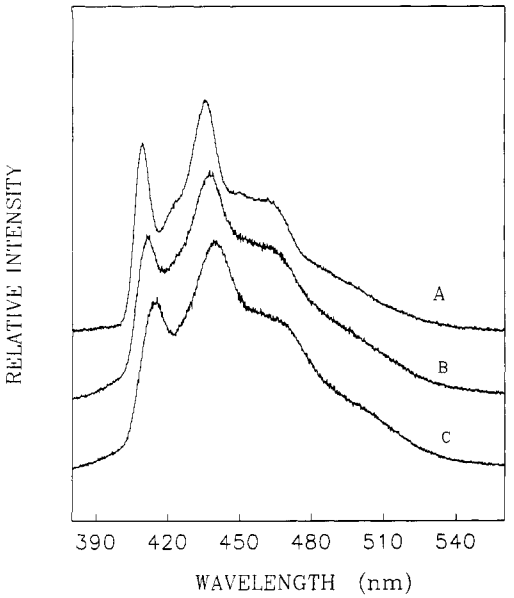

FIGURE 2: Phosphorescence spectra at 77 K of (A) NCp7·Zn, (B) NCp7·Zn + poly(U), and (C) NCp7·Zn + poly(I). See the text (Materials and Methods) for experimental details.

Table 1: Selected Triplet State Properties of NCp7·Zn and Its RNA and DNA Complexes

sample[b]	λ (nm)	τ (s)	ODMR freq[a] (GHz)		zfs parameter (GHz)	
			D–E	*2E*	*E*	*D*
NCp7·Zn	409.2	6.5 (92%) 1.8 (8%)	1.74	2.50	1.25	2.99
NCp7·Zn + poly(I)	415.1	4.9 (52%) 1.7 (48%)	1.62	2.55	1.28	2.89
NCp7·Zn + poly(U)	411.0	6.1 (65%) 2.2 (35%)	1.69	2.54	1.27	2.96
NCp7·Zn + poly(C)	410.6	5.7 (28%) 0.6 (72%)	1.7			
NCp7·Zn + poly(A)	410.4	5.7 (49%) 2.1 (56%)	1.6			
NCp7·Zn + poly(G)	413.6	4.6 (66%) 1.4 (34%)				
NCp7·Zn + dG_8	413.6	5.0 (57%) 1.3 (43%)	1.70	2.50	1.25	2.95
NCp7·Zn + poly(dT)	410.8	5.5 (65%) 2.0 (35%)				
NCp7·Zn + $(5\text{-BrdU})_7$dT[c]	418.4	0.22 (58%) 0.84 (36%) 3.3 (6%)				

[a] All ODMR frequencies listed were obtained using delayed slow passage (see text) and corrected for fast passage effects. Signals that are not listed are either weak or not observed. [b] Samples were excited at 295 nm with a 16 nm bandpass; the emission bandpass was 3 nm. T = 77 K for phosphorescence and lifetime measurements except where noted. ODMR measurements were made at 1.2 K. [c] Phosphorescence and lifetime measurements were made at 4.2 K.

Figure 3. The phosphorescence of the synthetic peptide is similar to that of NCp7·Zn (Figure 2A), suggesting that the tryptophan in the second zinc finger fragment is in a similar environment as that in NCp7·Zn. When complexed with RNA polymers, the phosphorescence shifts, listed in Table 2, are significantly smaller than the corresponding shifts in NCp7·Zn (Table 1), except for the poly(G) complex. The peptide/poly(G) complex exhibits a phosphorescence red-shift and lifetime reduction similar to those found in the NCp7·Zn/poly(G) complex. The phosphorescence lifetimes exhibit some reduction in the poly(I) complex, but not to the extent seen in the NCp7·Zn/poly(I) complex (compare Tables 1 and 2). The overall trends in phosphorescence red-shift and lifetime reduction observed for the synthetic second zinc finger peptide

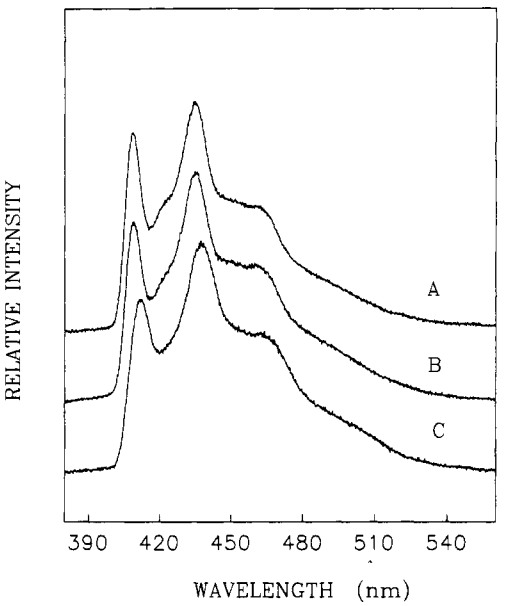

FIGURE 3: Phosphorescence spectra at 77 K of the synthetic second zinc finger peptide (A) and its complexes with (B) poly(U) and (C) poly(I). The concentration of the peptide was ca. 0.12 mM while that for the nucleotides was ca. 1.3 mM. Excitation was at 295 nm with a 16 nm bandpass; the emission bandpass was 3 nm.

Table 2: Selected Triplet State Properties of the Synthetic NCp7 Second Zinc Finger Peptide and Its RNA and DNA Complexes

sample[b]	λ (nm)	τ (s)	ODMR freq (GHz)[a]		zfs parameter (GHz)	
			D–E	*2E*	*E*	*D*
second zinc finger peptide	408.4	6.8 (70%) 4.8 (30%)	1.73	2.54	1.27	3.00
second zinc finger peptide + poly(I)	412.4	5.9 (71%) 2.8 (29%)	1.68	2.52	1.26	2.94
second zinc finger peptide + poly(U)	408.6	6.4 (85%) 2.6 (16%)	1.74	2.52	1.26	3.00
second zinc finger peptide + poly(G)	414.0	5.0 (76%) 1.5 (24%)				
second zinc finger peptide + $(5\text{-BrdU})_7$dT[c]	418.0	0.9 (43%) 0.2 (41%) 5.2 (16%)	1.62	2.60	1.30	2.92

[a] All ODMR frequencies are corrected for fast passage effects. Signals that are not listed are either weak or not observed. [b] Samples were excited at 295 nm with a 16 nm bandpass; the emission bandpass was 3 nm. T = 77 K for phosphorescence and lifetime measurements except where noted. ODMR measurements were made at 1.2 K. [c] Phosphorescence and lifetime measurements were made at 4.2 K.

complexes are similar to those found for NCp7·Zn, with the largest changes occurring with the poly(G) and poly(I) complexes (Table 2). An external HAE on Trp37 induced by the Br atom in the peptide/$(5\text{-BrdU})_7$dT complex was observed, as evidenced by the large lifetime reduction (Table 2).

The phosphorescence 0,0-band peak wavelengths and lifetimes of the synthetic carboxymethylated second zinc finger peptide and some of its RNA complexes are given in Table 3. This peptide has each of the cysteine residues of its zinc finger carboxymethylated, preventing the binding of zinc or the formation of disulfide bridges to produce a localized compact structure analogous to a zinc finger. For this peptide, the phosphorescence spectra exhibit no change in the presence of RNA. Also, the phosphorescence lifetimes were not significantly affected upon RNA binding. In its complexes with $(5\text{-BrdU})_7$dT and poly(5-HgU), however, large phosphorescence lifetime reductions typical of an external HAE were observed (Table 3). These substrates also induce a large phosphorescence red-shift (Table 3).

Table 3: Selected Triplet State Properties of the Synthetic Carboxymethylated NCp7 Second Zinc Finger Peptide and Its Solutions Containing RNA and DNA

sample[b]	λ (nm)	τ (s)	ODMR freq (GHz)[a] D–E	ODMR freq (GHz)[a] 2E	zfs parameter (GHz) E	zfs parameter (GHz) D
carboxymethylated peptide	409.0	6.1 (95%) 0.8 (4%)	1.74	2.56	1.28	3.02
carboxymethylated peptide + poly(I)	409.6	6.2 (81%) 2.1 (19%)	1.74	2.56	1.28	3.02
carboxymethylated peptide + poly(U)	409.2	6.4 (89%) 2.0 (11%)	1.73	2.56	1.28	3.02
carboxymethylated peptide + (5-BrdU)$_7$dT[c]	416.4	0.3 (44%) 1.4 (30%) 6.1 (26%)				
carboxymethylated peptide + poly(5-HgU)[d]	415.2	0.008 (59%) 0.061 (25%) 0.91 (15%)				

[a] All ODMR frequencies are corrected for fast passage effects. Signals that are not listed are either weak or not observed. [b] Samples were excited at 295 nm with a 16 nm bandpass; the emission bandpass was 3 nm. T = 77 K for phosphorescence and lifetime measurements except where noted. ODMR measurements were made at 1.2 K. [c] Phosphorescence and lifetime measurements were made at 4.2 K. [d] A $D+E$ ODMR signal at 4.29 GHz after correction for microwave sweep rates was observed along with weak D–E and $2E$ signals.

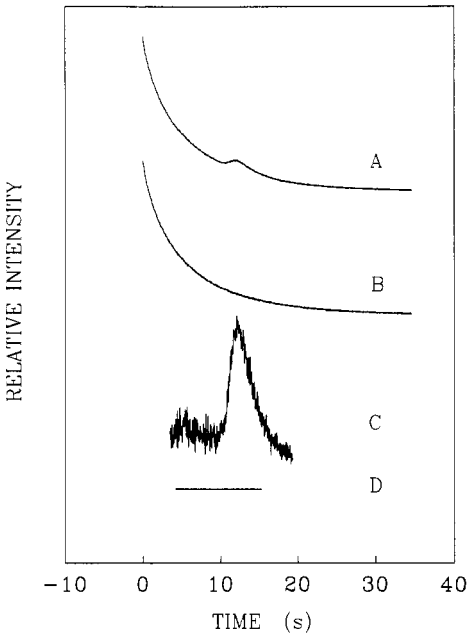

FIGURE 4: Delayed slow passage decay at 1.2 K of NCp7·Zn (A). A normal decay curve is shown in part B. After subtracting the normal decay curve (B) from the delayed slow passage decay (A), the resulting ODMR signal is shown (C). The straight line (D) indicates the time interval during which the microwaves were swept from 1.2 to 2 GHz through the D–E resonance. The spectra were signal averaged for eight scans.

ODMR Results. Since it was difficult to obtain steady-state ODMR signals from the NCp7·Zn/RNA complexes, a delayed slow passage ODMR technique was used to enhance the ODMR signal. In this case, however, the steady-state signal polarity information is lost. The delayed slow passage ODMR results (corrected for fast passage effects) for NCp7·Zn and its RNA and DNA complexes are listed in Table 1. Examples of this measurement are shown in Figures 4 and 5. The NCp7·Zn/poly(I) complex, in addition to having the most significant phosphorescence red-shift and lifetime reduction, also exhibits the largest reduction in the zfs D parameter. The D parameter is shifted by 100 MHz from 2.99 GHz in the uncomplexed NCp7·Zn to 2.89 GHz in the

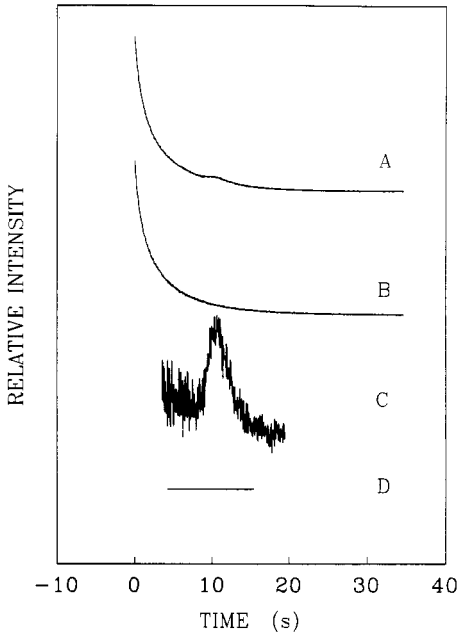

FIGURE 5: Delayed slow passage decay at 1.2 K of NCp7·Zn/poly(I) complex (A). A normal decay curve is shown in part B. After subtracting the normal decay curve (B) from the delayed slow passage decay (A), the resulting ODMR signal is shown (C). The straight line (D) indicates the time interval during which the microwaves were swept from 1.3 to 2.1 GHz through the D–E resonance. The spectra were signal averaged for eight scans.

NCp7·Zn/poly(I) complex. For the NCp7·Zn/poly(U) complex, the reduction in D is less, only 30 MHz. The NCp7·Zn/dG$_8$ complex also shows a smaller reduction in D of 40 MHz. The smaller reductions are marginally significant since the experimental error in D using the delayed slow passage technique is estimated to be ±20 MHz. For the other complexes, the zfs parameters could not be determined accurately because of the weak D–E and (especially) $2E$ signals. Despite the aforementioned low signal-to-noise ratio, steady-state ODMR performed on the RNA complexes showed positive signal polarity for the D–E and $2E$ ODMR transitions except for the NCp7·Zn/poly(I) and NCp7·Zn/dG$_8$ complexes. Steady-state slow passage ODMR spectra revealed a reversal in signal polarity of the D–E signal in the NCp7·Zn/poly(I) complex and of both the D–E and $2E$ signals in the NCp7·Zn/dG$_8$ complex relative to uncomplexed NCp7·Zn (Figure 6).

The slow passage ODMR results of the NCp7·Zn synthetic second zinc finger peptide and its RNA complexes are listed in Table 2. Its complex with poly(I) exhibits the largest reduction in D of 60 MHz. In Table 3, the slow passage ODMR results of the synthetic carboxymethylated second zinc finger peptide are shown. Here, the zfs parameters are unchanged relative to the uncomplexed peptide. When bound to (5-BrdU)$_7$dT, NCp7·Zn and both synthetic peptides exhibit heavy atom effects, indicating close range interactions between Trp37 and the Br-containing oligomer. In the case of NCp7·Zn and the NCp7·Zn synthetic second zinc finger peptide, such a heavy atom effect is consistent with the red-shift induced in the tryptophan phosphorescence when in the presence of unmodified RNA. Both effects suggest stacking interactions between Trp37 and the nucleobases. No red-shifts of the phosphorescence were found for the carboxymethylated zinc finger peptide, however, in the presence of RNA. Since a HAE was observed with (5-BrdU)$_7$dT, as well as with poly(5-HgU), it is possible that these result from specific interactions between Trp37 and the heavy atoms that are not characteristic of the interaction of the carboxy-

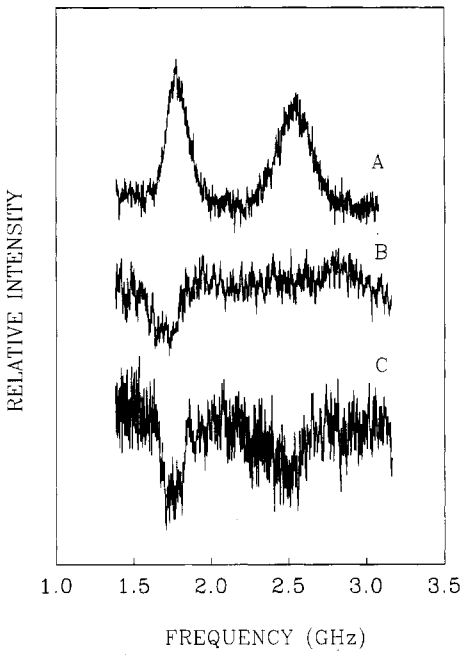

FIGURE 6: Steady-state slow passage ODMR spectra of (A) NCp7·Zn, (B) its complex with poly(I), and (C) its complex with dG_8. See the text (Materials and Methods) for experimental details. The ODMR signals are, from low to high frequencies, *D–E* and 2*E*, respectively. The microwave sweep rates were 33, 68, and 68 MHz/s for spectra A, B, and C, respectively. The spectra were signal averaged for 25, 100, and 100 scans for A, B, and C, respectively.

Table 4: Relative Sublevel Populating Rates for NCp7·Zn and Its RNA Complexes

sample[a]	P_x[b]	P_y[b]	P_z[b]
NCp7·Zn	≈0.37	≳0.45	≲0.18
NCp7·Zn + poly(I)	≳0.48	≲0.31	≲0.21
NCp7·Zn + poly(U)	≳0.41	≲0.35	≲0.24

[a] The relative sublevel populating rates were determined by a pulsed optical excitation microwave-induced delayed phosphorescence (POEMIDP) technique. In this case, the sample was excited for 100 ms, and a typical delay time of 70 ms elapsed before the microwave frequency was swept (100 GHz/s) through one of the transitions. [b] The values quoted are limiting values due to the presence of background phosphorescence from impurities and/or nucleotides.

methylated peptide with unmodified RNA.

Relative Sublevel Populating Rates and Apparent Sublevel Decay Constants. The relative populating rates for the three spin sublevels of Trp37 are listed in Table 4. These were obtained by means of pulsed optical excitation microwave-induced delayed phosphorescence (POEMIDP) experiments. A typical POEMIDP transient of the NCp7·Zn/poly(U) complex is shown in Figure 7. We observe that upon complex formation the relative populating rates for the T_x and, to a lesser extent, T_z sublevels of Trp37 are enhanced, whereas that for the T_y sublevel is reduced. The apparent sublevel decay constants for NCp7·Zn and its complexes, obtained from microwave-induced delayed phosphorescence (MIDP) experiments, are listed in Table 5. The sublevel decay constants are significantly enhanced upon complex formation. The largest enhancements occur in k_x, as clearly seen for the poly(I) complex of NCp7·Zn. These changes are consistent with the observed overall phosphorescence lifetime reduction upon formation of these complexes (Table 1).

DISCUSSION

The binding of RNA to NCp7·Zn affects the environment of Trp37 located on the C-terminal zinc finger as shown by the observed spectroscopic changes reported above. This is

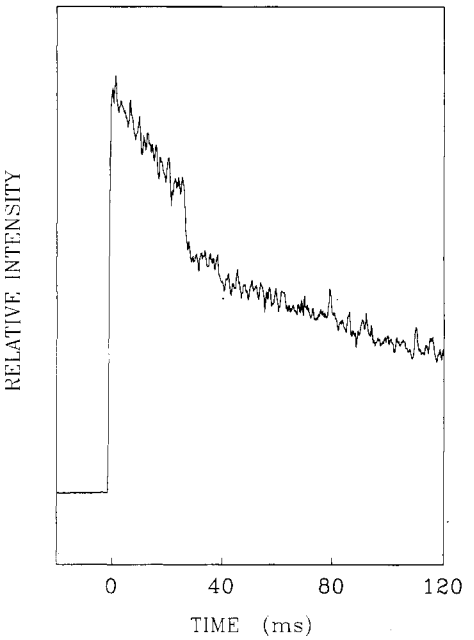

FIGURE 7: POEMIDP transient of the NCp7·Zn/poly(U) complex. Microwaves were swept from 1 to 2 GHz in 10 ms. Optical excitation time was 0.1 s. The spectrum was signal averaged for 40 scans.

Table 5: Apparent Sublevel Decay Constants for NCp7·Zn and Its RNA Complexes

sample[a]	k_x (s^{-1})	k_y (s^{-1})	k_z (s^{-1})
NCp7·Zn	0.41	0.052	0.086
NCp7·Zn + poly(I)	0.66	0.067	0.11
NCp7·Zn + poly(U)	0.49	0.062	0.051
NCp7·Zn + dG_8	0.56	0.20	0.091

[a] The sublevel apparent decay constants were determined using microwave-induced delayed phosphorescence (MIDP) techniques.

consistent with a recent NMR study that suggests interactions between the hydrophobic residues on the zinc finger and nucleic acid bases (South & Summers, 1993). The nature of these interactions has been investigated further in this study. The phosphorescence red-shifts and reductions in triplet lifetime that we observed for Trp37 are consistent with earlier studies on aromatic stacking interactions of tryptophan and quinoxaline with nucleic acid bases in which phosphorescence red-shifts, triplet lifetime reductions, and reductions in the *D* parameter were observed (Zang et al., 1987; Tsao et al., 1989; Alfredson et al., 1991a,b). The data presented in Table 1 show that the largest red-shift that we have observed occurs when NCp7·Zn is bound to poly(I). The red-shift of 5.9 nm measured in this study is somewhat larger than the ca. 4 nm red-shift experienced by Trp54 of *E. coli* SSB when bound to poly(dT) (Tsao et al., 1989). The magnitude of the phosphorescence red-shift is slightly less for NCp7·Zn binding to poly(G) and dG_8, which have a nucleobase similar to I. This is then followed by poly(U), poly(C), and poly(A), in that order. This ordering of the nucleic acid bases agrees with the rank of binding affinities of NCp7·Zn to model single-stranded DNA oligonucleotides as measured by fluorimetric equilibrium binding isotherms at 25 °C (Casas-Finet et al., 1993). In that study, the ordering of the affinity of NCp7·Zn to the bases is G > U > C > A. The two sets of data are compared in Figure 8. In this figure, the ordinate scales linearly with the binding free energy of NCp7·Zn. We have argued previously (Alfredson et al., 1991b) that the phosphorescence red-shift is expected to scale linearly with the contribution of the aromatic stacking interactions to the binding free energy. Thus, if contributions to the total binding energy other that tryptophan stacking were independent of

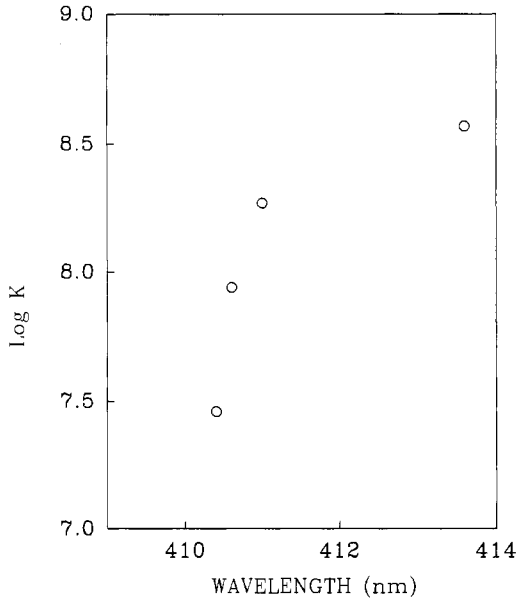

FIGURE 8: A semilogarithmic plot of the apparent affinity constants of NCp7·Zn for various DNA oligonucleotides determined from a fluorescence quenching study (Casas-Finet et al., 1993) against the phosphorescence 0,0-band peak wavelengths of NCp7·Zn/RNA complexes. The phosphorescence 0,0-band peak wavelengths, from blue to red, correspond to the complexes of NCp7·Zn with poly(A), poly(C), poly(U), and poly(G), respectively.

the nucleobase identity, a linear relation would be expected. In other words, a linear correlation between the phosphorescence red-shift and the binding free energy for different RNAs would imply that any base selectivity could be attributed to the aromatic stacking interactions. Since this is decidedly not the case for NCp7·Zn, we can conclude that contributions to complex stabilization other than aromatic stacking interactions depend on the identity of the RNA nucleobases. It appears, however, that the largest contribution of Trp37 stacking interactions to complex stabilization occurs for poly(I).

The reduction in triplet lifetime of Trp37 in NCp7·Zn that occurs when bound to RNA also varies with base in the same manner as the binding affinities. The largest reductions in lifetime occur with binding to poly(I) and poly(G), while binding to the other RNA's induce smaller reductions (Table 1). Reduction in triplet lifetimes of tryptophan is expected to accompany an increase in the polarizability of the environment. The (π, π^*) triplet states of aromatic molecules are mixed predominantly with (σ, π^*) and (π, σ^*) singlet states by spin–orbit coupling (McGlynn et al., 1969). The energy of these highly diffuse states is lowered by an increasingly polarizable environment, thus enhancing spin–orbit mixing.

For the synthetic second zinc finger peptide, the phosphorescence red-shifts upon binding poly(G), poly(I), and poly(U) are smaller than those seen for NCp7·Zn, but the trend is similar. The ranking of nucleobase-induced phosphorescence lifetime reduction agrees with that obtained for NCp7·Zn. Thus, the tryptophan in the second zinc finger peptide experiences similar, although smaller, changes in its environment compared to those of Trp37 in NCp7·Zn upon RNA binding. It also suggests that the zinc fingers function similarly in the synthetic peptide and in NCp7·Zn. For the synthetic carboxymethylated second zinc finger peptide, there is practically no shift in the phosphorescence 0,0-band when it is treated with poly(I) and poly(U). The phosphorescence lifetime also shows no significant reduction. This is in agreement with the known decrease in nucleic acid binding affinity for a metal-free zinc finger peptide (Delahunty et al., 1992).

The ODMR signals for NCp7·Zn are typical of normal tryptophans but they become much weaker in the RNA complexes. Trp37 exhibits a 100 MHz reduction of its D parameter in the poly(I) complex, which is significantly larger than the 40 MHz decrease observed in the poly(U) complex. In comparison, the reduction of the D value of Trp54 on binding *E. coli* SSB to poly(dT) is found to be ca. 280 MHz (Tsao et al., 1989). Again, these results correlate with the phosphorescence red-shifts and the lifetime reductions. One interesting observation shown in Figure 5 is that the D–E signal in the NCp7·Zn/poly(I) complex and both D–E and $2E$ ODMR signals in the NCp7·Zn/dG_8 complex are clearly of negative polarity in steady-state slow passage experiments. This contrasts with the positive polarity of the Trp37 ODMR signals in the free protein. Reversal in signal polarity is unusual, but it has been observed previously for tryptophan in the *E. coli* SSB complex with poly(dT) in which Trp54 undergoes a polarity reversal of its ODMR signals (Zang et al., 1987; Tsao et al., 1989). Polarity reversals of ODMR signals are also found for quinoxaline and quinoline chromophores in bis-intercalating peptide antibiotics upon being bound to DNA (Alfredson et al., 1989, 1991a,b). In each case, the chromophore undergoes aromatic stacking interactions with the nucleic acid bases. Thus, the observation of a signal polarity reversal is yet another indication of aromatic stacking interactions of Trp37 with the nucleobases. The zfs parameters for the other NCp7·Zn complexes could not be determined because of significant interfering background phosphorescence from the base (as in poly(G), and in poly(A) to some extent) or because of very weak ODMR signal-to-noise ratio. For the synthetic second zinc finger peptide, the magnitude of the observed reduction in D is smaller (60 MHz compared with 100 MHz) than that of NCp7·Zn when bound to poly(I). No reduction in D is observed in its complex with poly(U). These observations, along with the smaller red-shifts in phosphorescence, suggest that the second zinc finger peptide alone has less affinity for RNA than NCp7·Zn, which has two zinc finger domains. In fact, this conclusion is consistent with our fluorescence titration results (Casas-Finet et al., unpublished) and with those from two recent studies. One suggests that the two zinc fingers are not functionally equivalent (Gorelick et al., 1993), and the other suggests that there is cooperative binding between the two fingers to RNA (Sakaguchi et al., 1993). The synthetic carboxymethylated second zinc finger peptide, which cannot form a zinc finger structure, exhibits no change in the zfs parameters upon addition of RNA. This, in combination with the phosphorescence results, suggests no change in Trp37 environment upon binding of the peptide to RNA under comparable experimental conditions. As mentioned earlier, heavy atom effects that are induced when this peptide binds to the heavy-atom-derivatized nucleic acids may be the result of specific interactions between the heavy atom and Trp37 that do not characterize interactions with unmodified nucleic acids. These results suggest that, for the apo zinc finger peptide, stacking interaction of Trp37 with nucleobases does not occur.

To characterize further the interaction between NCp7·Zn and the RNA polymers, relative triplet sublevel populating rates were measured. As seen in Table 4, complex formation with poly(I) and poly(U) results in the enhancement of populating rate for the T_x sublevel relative to that of the T_y sublevel, while the relative sublevel populating rate of T_z is slightly enhanced. When bound to poly(dT), Trp54 of *E. coli* SSB undergoes an extremely large relative enhancement of the T_x sublevel populating rate (Zang et al., 1987) a factor that is largely responsible for the reversal of steady-state signal

polarity. In a normal tryptophan triplet state, the radiative T_x sublevel is the least populated in the photostationary state, resulting in a positive ODMR signal when it is in resonance with either of the nonradiative sublevels. Thus, an enhanced P_x and a reduced P_y could produce a smaller population difference between T_x and the other sublevels in the steady state. In some complexes, as seen in the NCp7·Zn/poly(I) complex and the NCp7·Zn/dG_8 complex, inverted polarity signals could result as they do also for Trp54 in *E. coli* SSB bound to poly(dT). For the tightly bound complexes, the apparent sublevel decay constants all show increases, especially of the T_x sublevel, as seen in Table 5. This, in conjunction with the increase in the relative T_x populating rate, may provide an explanation for the difficulty in observing steady-state slow passage ODMR. Note that a large reduction by a factor of 4 of the T_x lifetime of Trp54 in the *E. coli* SSB complex has been associated with stacking interaction with the nucleobases of poly(dT) (Tsao et al., 1989).

In a previous study, we have suggested that stacking interactions occur between Trp37 of NCp7·Zn and a heavy-atom-derivatized RNA [poly(5-HgU)] based on the observation of an external HAE on Trp37 (Lam et al., 1993). In this study, we have extended the investigation to unmodified RNA homopolymers and have presented results that suggest the presence of aromatic stacking interactions between NCp7·Zn and unmodified RNA nucleobases. The extent of the spectroscopic effects associated with stacking show a correlation with the affinity of NCp7·Zn to the RNA bases, suggesting that aromatic stacking interactions contribute significantly toward stabilization of NCp7·Zn/RNA interactions. Such a correlation between triplet state spectroscopic effects relating to stacking and the affinity of peptide–nucleic acid binding is demonstrated by recent studies of the binding of the bis-intercalating quinoxaline antibiotic echinomycin and of its quinoline-substituted analog, 2QN, to various DNAs (Alfredson et al., 1989, 1991b). In these studies, the reduction of the D parameter of the intercalated aromatic, quinoxaline or quinoline, was found to correlate linearly with the free energy of drug–DNA binding.

A recent fluorescence study (Mely et al., 1993) concluded that stacking interactions occur between tRNA and two NCp7-related peptides, one the N-terminal zinc finger domain and the other the C-terminal zinc finger domain. Thus, our work provides additional evidence that aromatic stacking interactions play a role in NCp7·Zn interactions with RNA, in addition to other factors such as electrostatic interactions between charged residues and hydrogen bonding.

REFERENCES

Alfredson, T. V., Maki, A. H., & Waring, M. J. (1989) *Biochemistry 29*, 9052–9064.

Alfredson, T. V., Lam, W.-C., Maki, A. H., & Waring, M. J. (1991a) *Appl. Mag. Res. 2*, 159–178.

Alfredson, T. V., Maki, A. H., & Waring, M. J. (1991b) *Biochemistry 30*, 9665–9675.

Bess, J. W., Jr., Powell, P. A., Issaq, H. J., Schumack, L. J., Grimes, M. K., Henderson, L. E., & Arthur, L. O. (1992) *J. Virol. 66*, 840–847.

Casas-Finet, J. R., Sowder, R. C., II, Sakaguchi, K., Appella, E., Henderson, L. E., & Erickson, J. W. (1993) *Biophys. J. 64*, A178.

Delahunty, M. D., South, T. L., Summers, M. F., & Karpel, R. K. (1992) *Biochemistry 31*, 6461–6469.

Dorfman, T., Luban, J., Goff, S. P., Haseltine, W. A., & Göttlinger, H. G. (1993) *J. Virol. 67*, 6159–6169.

Gorelick, R. J., Nigida, S. M., Bess, J. W., Arthur, L. O., Henderson, L. E., & Rein, A. (1990) *J. Virol. 64*, 3207–3211.

Gorelick, R. J., Chabot, D. J., Rein, A., Henderson, L. E., & Arthur, L. O. (1993) *J. Virol. 67*, 4027–4036.

Henderson, L. E., Sowder, R. C., Copeland, T. D., Oroszlan, S., & Benveniste, R. E. (1990) *J. Med. Primatol. 19*, 411–419.

Henderson, L. E., Bowers, M. A., Sowder, R. C., II, Serabyn, S. A., Johnson, D. G., Bess, J. W., Jr., Arthur, L. O., Bryant, D. K., & Fenselau, C. (1992) *J. Virol. 66*, 1856–1865.

Hershberger, M. V., Maki, A. H., & Galley, W. C. (1980) *Biochemistry 19*, 2204–2209.

Hoff, A. J. (1989) in *Advanced EPR. Applications in Biology & Biochemistry* (Hoff, A. J., Ed.) pp 633–684, Elsevier, Amsterdam.

Kwiram, A. L. (1982) in *Triplet State ODMR Spectroscopy* (Clarke, R. H., Ed.) pp 428–478.

Lam, W.-C., Maki, A. H., Casas-Finet, J. R., Erickson, J. W., Sowder, R. C., II, & Henderson, L. E. (1993) *FEBS Lett. 328*, 45–48.

Maki, A. H. (1984) in *Biological Magnetic Resonance* (Berliner, L., & Reuben, J., Eds.) Vol. 6, pp 187–293, Plenum Press, New York.

McGlynn, S. P., Azumi, T., & Kinoshita, M. (1969) *Molecular Spectroscopy of the Triplet State*, Prentice-Hall, Englewood Cliffs, NJ.

Mely, Y., Piemont, E., Sorinas-Jimeno, M., de Rocquigny, H., Julian, N., Morellet, N., Roques, B. P., & Gerard, D. (1993) *Biophys. J. 65*, 1513–1522.

Michelson, A. M., Dondon, J., & Grunberg-Manago, M. (1962) *Biochim. Biophys. Acta 55*, 529–540.

Sakaguchi, K., Zambrano, N., Baldwin, E. T., Shapiro, B. A., Erickson, J. W., Omichinski, J. G., Clore, G. M., Gronenborn, A. M., & Appella, E. (1993) *Proc. Natl. Acad. Sci. U.S.A. 90*, 5219–5223.

Schmidt, J., Veeman, W. S., & van der Waals, J. H. (1969) *Chem. Phys. Lett. 4*, 341–345.

South, T. L., & Summers, M. F. (1993) *Protein Sci. 2*, 3–19.

South, T. L., Blake, P. R., Sowder, R. C., Arthur, A. O., Henderson, L. E., & Summers, M. F. (1990) *Biochemistry 29*, 7768–7789.

Summers, M. F. (1990) *Biochemistry 29*, 7768–7789.

Summers, M. F., Henderson, L. E., Chance, M. R., Bess, J. W., Jr., South, T. L., Blake, P. R., Sagi, I., Perez-Alvarado, G., Sowder, R. C., II, Hare, D., & Arthur, L. O. (1992) *Protein Sci. 1*, 563–574.

Tsao, D. H. H., Casas-Finet, J. R., Maki, A. H., & Chase, J. W. (1989) *Biophys. J. 55*, 927–936.

Ts'o, P. O. P., Rapaport, S. A., & Bollum, F. J. (1966) *Biochemistry 5*, 4153–4169.

Zang, L.-H., Maki, A. H., Murphy, J. B., & Chase, J. W. (1987) *Biophys. J. 52*, 867–872.